Journal of Applied Research in Science and Humanities

Monitoring variations in blood flow using Mathematica software: Study on coronary artery

Hamed M. Sayed[1], **Hagar E Mohamed**, **Mariam Y Bostan**, **Mariam W. ElSayed**, **Mariam R. Shorba**, **Menna A. Mohamed**, **Nesma Kh. Abdelfattah**, **and Yara Kh. Serag**

Department of Mathematics, Faculty of Education, Ain Shams University, Roxy, Cairo, Egypt

Abstract

This project examines the rheological characteristics of a non-Newtonian Casson nanofluid model for blood flow through artery constriction with a catheter that has mild wall stenosis and central blood thrombus. Heat generation, first-order chemical reactions, and first and second order velocity slip conditions are all considered, along with modeling the blood flow. Implementing the analytical solution using Mathematica programming tools yields analytical expressions for velocity distribution, temperature distribution, concentration distribution, wall shear stress, and heat transfer coefficient. A graphic representation of the results is provided.

Keywords

Stenosis artery, Catheter, Non Newtonian model, Slip flow, Nanofluid, Heat generation, Chemical reaction.

1. Introduction

A serious health danger is arterial stenosis, which is defined by the narrowing of arteries brought on by the buildup of lipids and other materials. Heart attacks and strokes are among the major cardiovascular problems that can arise from this illness, which restricts blood circulation. Understanding how blood moves through constricted arteries is a useful way to address this problem, particularly when taking into account elements like the presence of plaques, clots, and the use of medical devices like catheters. Heart illnesses, including ischemia, atherosclerosis, and angina pectoris, are among the world's leading causes of death. Ischemia is a brief deficiency of

[1] Corresponding author. E-mail: hamedali@edu.asu.edu.eg

oxygen in a particular part of the body, frequently brought on by a blockage or narrowing (stenosis) in the blood vessel supplying that region. Stenosis is the abnormal constriction of an artery, usually brought on by the buildup of fatty deposits, which affects a number of blood flow-related systems. This disorder causes the inner walls of arteries to constrict or narrow. It is a major contributor to the onset of dangerous conditions, including atherosclerosis. Thus, it is useful to study blood flow in a stenotic artery in order to comprehend circulatory problems [1-3].

The thin, flexible, tubular device known as a catheter is used to occlude a vessel or enter or withdraw fluids. Interventional radiology uses fluoroscopic imaging to guide catheters in order to detect and treat vascular disorders. A catheter can be inserted into an artery, for example, to check for stenosis or arterial occlusions. Thrombectomy operations use specialized catheters that are fitted with tools to break up and extract blood clots. Likewise, percutaneous transluminal angioplasty increases blood flow by dilatation of constricted or blocked arteries using balloon-tipped catheters. Kanai et al. [4] noted that the insertion of a catheter increased the pressure. Coaxial tubes are used to simulate blood as Newtonian fluid, with the catheter representing the inner tube and the artery the outer tube. Many studies [5–7] have attempted to describe the dynamics of blood flow in annular geometries that are frequently found in catheterized stenotic arteries.

Fluids stick to surfaces, according to a common notion in fluid mechanics known as the no-slip condition, where the body and fluid particles have the same instantaneous velocity [8]. In certain physical situations, such as when a liquid spreads on a solid substrate or when polymer melts are extruded from a capillary tube, the no-slip presumption is no longer applicable, and the no-slip boundary condition must be exchanged by a slip boundary condition. For technologies like internal cavities and the polishing of prosthetic heart valves, fluids that permit slippage are crucial. At low flows, the linear navier's slip condition performs well. The Navier's slip condition fails with greater flows, though, as the slip length quickly grows. In order to address this, researchers created second-order slip boundary conditions, which are used to simulate rarefied gas flows and microscale gas fluxes [9]. Yasin et al. [10] examined how steady boundary layer flow and heat transfer are affected by second-order velocity slip over a permeable shrinking sheet submerged in a porous medium. A second-order momentum slip model over an exponential stretching sheet was used to investigate the physical significance of activation energy in binary chemical reactions [11]. The second slip condition in mathematical modelling frequently entails higher-order corrections and includes a slip velocity proportionate to the shear stress at the wall. In fields such as vacuum technology, aeronautical engineering, and Micro-Electro-Mechanical Systems design, it enhances the precision of simulations and forecasts. Designing effective systems in which gas-surface interactions are crucial requires an understanding of and adherence to the second slip condition [12]. Sahoo and Nandkeolyar [12] analyzed the generation of entropy in the magnetohydrodynamic second-order slip flow of a Casson nanofluid over a horizontal stretching sheet within a non-Darcy porous medium, where nonlinear thermal radiation and Hall current predominate. Sayed et al. [13] investigated heat transmission analysis of Casson nanofluid flow with second-slip conditions using kerosene oil-suspended Al2O3 or GO nanoparticles and single and multi-walled carbon nanotubes.

Nanofluids represent a type of fluid composed of a base liquid and nanoparticles, initially introduced by Choi [14]. Nanoparticles with biochemical applications are commonly utilized in various medical treatment processes [15]. The proposed technique seeks to improve the thermal conductivity of the base fluid by integrating solid nanoparticles that possess high thermal conductivity [16]. A mathematical model for analyzing red blood cells loaded with nanoparticles in blood has been created for a stenotic catheterized artery [17]. In an obliquely skewed artery, the electro-osmotic ionic Rabinowitsch blood flow carrying gold and graphene oxide nanoparticles is studied by Paul and Das [18]. Analyzing the MHD bioconvection peristaltic motion of Reiner-Philippoff nanofluid along a curved channel was done using a new artificial neural network model [19]. Ghasemi and Ranjbar [20] examined the peristaltic flow of nanofluids across a wavy channel, which has important uses in blood pumps and pharmacological drug delivery systems.

The Casson fluid model, a non-Newtonian fluid model with yield stress, is frequently used to simulate blood flow via constricted arteries. The flow of blood in stenotic arteries at low shear rates has been mathematically modeled by numerous researchers using the Casson fluid model. Casson [21] examined the Casson fluid model's validity in his study on blood flow properties and found that blood shows a non-zero yield stress at low shear rates. The Casson fluid model is appropriate for depicting the simple shear behavior of blood in tiny arteries [22,23]. Sharma et al. [24] have investigated the reduction of entropy generation in an inclined artery with a superposed barrier by combining Au-Cu/blood hybrid nanoparticles with a non-Newtonian Casson fluid whose viscosity depends on the hematocrit rate. Dhinakaran et al. [25] have explored a vertically narrow artery to propel Cu-Al2O3/blood visco-plastic hybrid nanofluids upward. In this study, the impact of magnetohydrodynamics on their behavior is examined.

Thus, the goal is to study the flow of a non-Newtonian nanofluid by anticipating its rheological characteristics using the Casson model while incorporating variables like the source of heat parameter, the first-order chemical reaction parameter, and the first and second slip parameters. In order to investigate the flow of nanofluid through a catheterized artery with stenosis, a thorough analysis of several relevant physical factors is being conducted. One specific goal is to investigate the nanofluid model to thoroughly study the physical effects on the flow. Utilizing analytical techniques aided by the Mathematica software, the issue is solved, and the results are graphically presented for various flow characteristics, such as the coefficient of thermal transfer and the shear stress.

2. The physical problem's description

Let us consider a mathematical model of steady, incompressible blood flow with (Au) metallic nanoparticles. Table 1 provides the nanoliquid's thermo-physical characteristics. The flow is limited to the annular space between two L-long coaxial tubes. An axial axis of $\tilde{z}$, which corresponds to the direction of blood movement, and a radial axis of $\tilde{r}$, which is oriented radially, are used to simulate blood circulation in this annulus. Blood flow via the artery is presumed to be axisymmetric, which means that flow properties vary independently of azimuthal angle. The wall of the inner tube has a colt, while the outer tube has mild stenosis that is axially symmetric, as shown in Fig. 1 . $\bar{\eta}(\bar{z})$ and $\bar{\epsilon}(\bar{z})$, respectively, define the outer and inner walls

$$\bar{\eta}(\bar{z}) = R\left[1 - k^{*}\left(b^{(n-1)}(\bar{z}-a) - (\bar{z}-a)^{n}\right)\right],\ a \le \bar{z} \le a+b, \quad (1)$$
$$= R,\ \text{otherwise},$$

$$\bar{\epsilon}(\bar{z}) = R\left[c + \sigma e^{-\pi^{2}(\bar{z}-\bar{z}_{d}-0.5)^{2}}\right],\ a \le \bar{z} \le a+b, \quad (2)$$
$$= cR,\ \text{otherwise}.$$

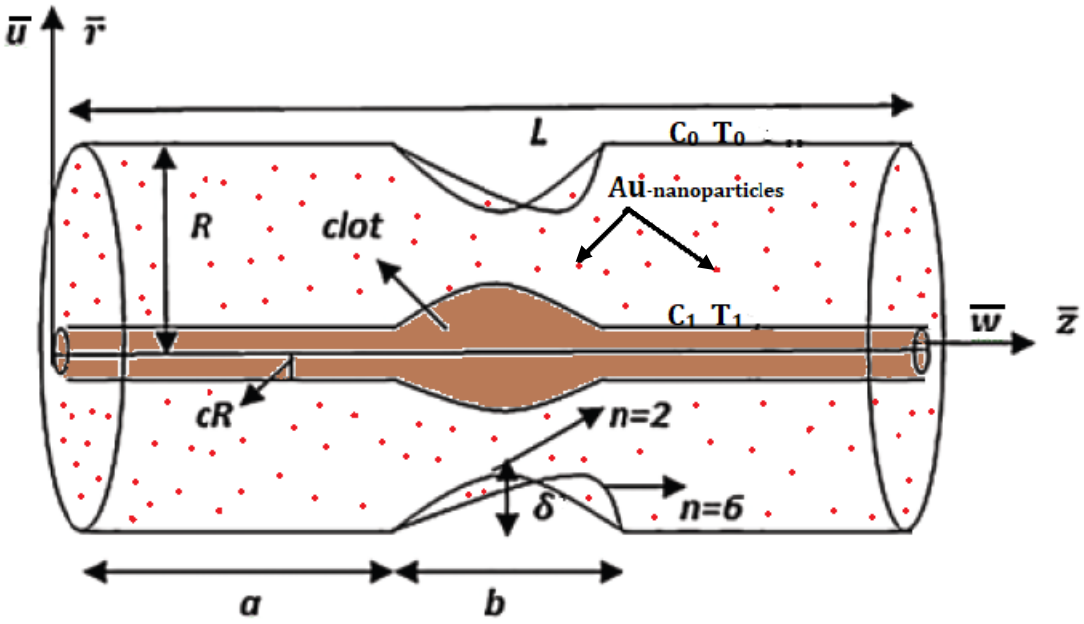

Fig. 1. Model schematic diagram.

Here, b stands for the length of the stenosis and R for the artery's radius in the non-stenotic region. The stenosis's shape is described by the parameter $n \geq 2$, and its location is indicated by a. The shape of the stenosis is symmetrical for $n = 2$, but it becomes non-symmetrical for $n = 6$. The constant k's value is given by

$$k^{*} = \frac{\bar{\delta}}{R\, b^{n}} \frac{n^{\frac{n}{n-1}}}{n-1}. \quad (3)$$

In which the maximum height of the stenosis at point $\bar{z} = a + \frac{b}{n^{\frac{1}{n-1}}}$ is represented by $\bar{\delta}$, while the maximum height of the thrombus at point $\bar{z} = \bar{z}_{d} + 0.5$ is represented by σ. The inner radius of the catheter is denoted by cR, where $c \ll 1$, while z_{d} indicates the thrombus's axial displacement.

A non-Newtonian nanofluid (a Casson Au/blood nanofluid) flowing steadily and incompressibly through a mildly stenosed artery with a catheter and a thrombus is described by the governing equations. The equations for momentum, energy, and concentration of the nanofluid in the

presence of chemical reaction, heat generation, and slip effects are provided by Fahim et al. [26] under the aforementioned assumptions.

$$\frac{\partial \bar{u}}{\partial \bar{r}} + \frac{\partial \bar{w}}{\partial \bar{z}} + \frac{\bar{u}}{\bar{r}} = 0, \tag{4}$$

$$\rho_{nf}\left(\bar{u}\,\frac{\partial \bar{w}}{\partial \bar{r}} + \bar{w}\,\frac{\partial \bar{w}}{\partial \bar{z}}\right) = -\frac{\partial \bar{p}}{\partial \bar{z}} + \mu_{nf}\left(1 + \frac{1}{\beta}\right)\left(\frac{\partial^2 \bar{w}}{\partial \bar{r}^{\,2}} + \frac{1}{\bar{r}}\,\frac{\partial \bar{w}}{\partial \bar{r}} + \frac{\partial^2 \bar{w}}{\partial \bar{z}^2}\right), \tag{5}$$

$$\rho_{nf}\left(\bar{u}\,\frac{\partial \bar{u}}{\partial \bar{r}} + \bar{w}\,\frac{\partial \bar{u}}{\partial \bar{z}}\right) = -\frac{\partial \bar{p}}{\partial \bar{r}} + \mu_{nf}\left(1 + \frac{1}{\beta}\right)\left(\frac{\partial^2 \bar{u}}{\partial \bar{r}^2} + \frac{1}{\bar{r}}\,\frac{\partial \bar{u}}{\partial \bar{r}} - \frac{\bar{u}}{\bar{r}^2} + \frac{\partial^2 \bar{u}}{\partial \bar{z}^2}\right), \tag{6}$$

$$(\rho c_p)_{nf}\left(\bar{u}\,\frac{\partial T}{\partial \bar{r}} + \bar{w}\,\frac{\partial T}{\partial \bar{z}}\right) = k_{nf}\left(\frac{\partial^2 T}{\partial \bar{r}^2} + \frac{1}{\bar{r}}\,\frac{\partial T}{\partial \bar{r}} + \frac{\partial^2 T}{\partial \bar{z}^2}\right) + Q_0(T - T_1), \tag{7}$$

$$\left(\bar{u}\,\frac{\partial C}{\partial \bar{r}} + \bar{w}\,\frac{\partial C}{\partial \bar{z}}\right) = D_{nf}\left(\frac{\partial^2 C}{\partial \bar{r}^2} + \frac{1}{\bar{r}}\,\frac{\partial C}{\partial \bar{r}} + \frac{\partial^2 C}{\partial \bar{z}^2}\right) - K(C - C_1). \tag{8}$$

The appropriate boundary conditions are

$$\bar{w} = \bar{w}_0 + \mu_{nf}\left(1 + \frac{1}{\beta}\right)\left(a_1\frac{\partial \bar{w}}{\partial \bar{r}} + b_1\frac{\partial^2 \bar{w}}{\partial \bar{r}^2}\right),\ T = T_0, \text{ and } C = C_0 \quad \text{at } \bar{r} = \bar{\eta},$$

$$\bar{w} = 0, T = T_1, \text{ and } C = C_1 \quad \text{at } \bar{r} = \bar{\epsilon}. \tag{9}$$

The components of axial and radial velocity are denoted by $\bar{w}$ and $\bar{u}$, respectively, and T is the nanoblood's temperature, C is its concentration, in equations (4)-(8). Fluid pressure is denoted by $\bar{p}$, while Q_0 and K stand for heat generation, and chemical reaction, correspondingly. Casson fluid parameter is denoted by β. Newtonian fluid is specified for $\beta \to \infty$, whereas non-Newtonian fluid is represented by $\beta \neq 0$. The heat transfer is accounted for by specifying T_o and T_1 as the temperatures at the artery wall and the catheter, respectively and C_0 and C_1 are the concentration at the wall of the artery and catheter, respectively.

Table 1 Refer to [27] for the thermophysical characteristics of the blood and Au nanoparticles.

Properties	**SI units**	**Blood**	**Gold (Au)**
Density ($\boldsymbol{\rho}$)	kg m^{-3}	1063	19320
Thermal conductivity (k)	W m^{-1} K^{-1}	0.492	314
Heat capacity (c_p)	J k^{-1} g^{-1} K^{-1}	3594	129
Prandtl number (Pr)		21	---

For the proposed nanofluid model, the thermophysical characteristics of blood, Au, and nanofluid are represented by the symbols (f, s, nf), orderly. The Au nanoparticles' solid volume fraction is symbolized by φ.

$$\frac{\rho_{nf}}{\rho_f} = (1-\varphi) + \varphi\frac{\rho_s}{\rho_f}, \tag{10}$$

$$\frac{\mu_{nf}}{\mu_f} = (1-\varphi)^{-2.5}, \tag{11}$$

$$\frac{(\rho c_p)_{nf}}{(\rho c_p)_f} = (1-\varphi) + \varphi\frac{(\rho c_p)_s}{(\rho c_p)_f}, \tag{12}$$

$$\frac{k_{nf}}{k_f} = \frac{(k_s - k_{nlr})\varphi k_{nlr}(y_2{}^2 - y_1{}^2 + 1) + (k_s + k_{nlr})y_2{}^2(\varphi y_1{}^2(k_{nlr} - k_f) + k_f)}{y_2{}^2(k_s + k_{nlr}) - (k_s - k_{nlr})\varphi(y_2{}^2 - y_1{}^2 + 1)},$$

$$\text{in which } k_{nlr} = 3k_f, y_2 = 1 + \frac{N_h}{2N_r}, y_1 = 1 + \frac{N_h}{N_r}, \tag{13}$$

$$\frac{D_{nf}}{D_f} = 1 - \phi. \tag{14}$$

The symbols N_r, N_h, and k_{nlr} refer, respectively, to the diameter of the nanoparticle, the thickness of the interfacial nanoparticle, and the interfacial thermal conductivity. The symbols (μ, D) represent ordered dynamic viscosity and thermal diffusivity.

To simplify the governing equations, we introduce the following dimensionless quantities and approximations

$$r = \frac{\bar{r}}{R},\ z = \frac{\bar{z}}{L}, w = \frac{\bar{w}}{u_0},\ p = \frac{R^2\,\bar{p}}{\mu_f\,u_0\,L},\ u = \frac{L\,\bar{u}}{\bar{\delta}u_0},\ \phi = \frac{C-C_1}{C_0-C_1}, \theta = \frac{T-T_1}{T_0-T_1},\ Re = \frac{\rho_f\,u_0 R}{\mu_f},$$
$$\delta = \frac{\bar{\delta}}{R},\ \varepsilon = \frac{R}{L}, h = \frac{a}{b},\ Le = \frac{\mu_f}{D_f\,\rho_f},\ Pr = \frac{(C_p)_f\,\mu_f}{K_f}, \beta_s = \frac{Q_0 R^2}{(T_0-T_1)K_f}, \gamma = \frac{KR^2}{D_f}, \tag{15}$$

where u_0 is the averaged velocity over the section of the channel of width R, β_s is the nondimensional heat source parameter with respect to fluid, γ is the chemical reaction parameter, Re is the Reynolds number, Pr is the Prandtl number, Le is the Lewis number, θ is the temperature, and ϕ is the concentration.

Then the equations (4)-(8) can be reduced to

$$\delta\,\frac{\partial u}{\partial r} + \frac{\partial w}{\partial z} + \delta\,\frac{\partial u}{\partial r} = 0, \tag{16}$$

$$\frac{\rho_{nf}}{\rho_f} Re\,\varepsilon^2\left(\delta\,u\frac{\partial w}{\partial r} + w\frac{\partial w}{\partial z}\right) = -\frac{\partial p}{\partial r} + \frac{\mu_{nf}}{\mu_f}\left(1+\frac{1}{\beta}\right)\left(\frac{\partial^2 w}{\partial r^2} + \frac{1}{r}\,\frac{\partial w}{\partial r} + \varepsilon^2\,\frac{\partial^2 w}{\partial z^2}\right), \tag{17}$$

$$\frac{\rho_{nf}}{\rho_f}\,Re\,\delta\,\varepsilon^3\left(\delta\,u\frac{\partial u}{\partial r} + w\frac{\partial w}{\partial z}\right) = -\frac{\partial p}{\partial r} + \frac{\mu_{nf}}{\mu_f}\left(1+\frac{1}{\beta}\right)\delta\,\varepsilon^2\left(\frac{\partial^2 u}{\partial r^2} + \frac{1}{r}\,\frac{\partial u}{\partial r} - \frac{u}{r^2} + \varepsilon^2\,\frac{\partial^2 u}{\partial z^2}\right), \tag{18}$$

$$\Pr \varepsilon \left(\delta\, u \frac{\partial \theta}{\partial r} + w \frac{\partial \theta}{\partial z}\right) = \frac{(\rho c_p)_f}{(\rho c_p)_{nf}} \frac{k_{nf}}{k_f} \left(\frac{\partial^2 \theta}{\partial r^2} + \frac{1}{r} \frac{\partial \theta}{\partial r} + \varepsilon^2 \frac{\partial^2 \theta}{\partial z^2}\right) + \beta_s \frac{(\rho c_p)_f}{(\rho c_p)_{nf}} \theta, \tag{19}$$

$$ReLe\, \varepsilon^2 \left(\delta u \frac{\partial \phi}{\partial r} + w \frac{\partial \phi}{\partial z}\right) = \frac{D_{nf}}{D_f} \left(\frac{\partial^2 \phi}{\partial r^2} + \frac{1}{r} \frac{\partial \phi}{\partial r} + \varepsilon^2 \frac{\partial^2 \phi}{\partial z^2}\right) - \gamma\, \phi. \tag{20}$$

For mild stenosis we can apply the condition $\delta \ll 1$ and taking extra condition $\varepsilon \sim O(1)$, then the equations (16)-(20) becomes

$$\frac{\partial w}{\partial z} = 0 \rightarrow w = w(r), \tag{21}$$

$$-\frac{\partial p}{\partial z} + \frac{\mu_{nf}}{\mu_f}\left(1 + \frac{1}{\beta}\right)\left(\frac{\partial^2 w}{\partial r^2} + \frac{1}{r}\frac{\partial w}{\partial r}\right) = 0, \tag{22}$$

$$\frac{\partial p}{\partial r} = 0 \rightarrow p = p(z), \tag{23}$$

$$\frac{k_{nf}}{k_f} \left(\frac{\partial^2 \theta}{\partial r^2} + \frac{1}{r} \frac{\partial \theta}{\partial r}\right) + \beta_s \theta = 0, \tag{24}$$

$$\frac{D_{nf}}{D_f} \left(\frac{\partial^2 \phi}{\partial r^2} + \frac{1}{r} \frac{\partial \phi}{\partial r}\right) - \gamma \phi = 0. \tag{26}$$

Then there exist a unique solution of the problem satisfying the nondimensional boundary conditions:

$$w = w_0 + \frac{\mu_{nf}}{\mu_f} \left(1 + \frac{1}{\beta}\right)\left(A \frac{\partial w}{\partial r} + B \frac{\partial^2 w}{\partial r^2}\right), \theta = 0, \phi = 0 \text{ at } r = \eta,$$

$$w = 0, \theta = 1, \phi = 1 \text{ at } r = \epsilon. \tag{27}$$

where $A = \frac{a}{R}$ is the dimensionless first-order velocity slip and $B = \frac{b}{R^2}$ is the dimensionless second-order velocity.

As well $\eta(z)$ and $\epsilon(z)$ in the dimensionless form become

$$\eta(z) = 1 - \delta \frac{n^{\frac{n}{n-1}}}{n-1}[(z - h) - (z - h)^n], \; h \le z \le h + 1,$$
$$= 1, \; otherwise, \tag{28}$$

$$\epsilon(z) = c + \sigma e^{-\pi^2 (z - z_d - 0.5)^2}, \; h \le z \le h + 1,$$
$$= c, \; otherwise. \tag{29}$$

3. Exact Solution

The axial velocity, temperature, and concentration can be computed (by using the command DSolve[eqn, y, x]) in the following manner by applying the appropriate boundary conditions (27) after the analytical solution of the axial velocity, temperature, and concentration is determined from equations (21)–(26):

$$\begin{aligned} w = {} & \frac{1}{4a_1(\eta^2\log(\epsilon) - \eta^2\log(\eta) - Ba_1 + A\eta a_1)}(-4w_0\eta^2\log(r)\,a_1 \\ & + 4w_0\eta^2\log(\epsilon)\,a_1 \\ & + \frac{\partial p}{\partial z}(-\epsilon^2\eta^2\log(r) + \eta^4\log(r) + r^2\eta^2\log(\epsilon) - \eta^4\log(\epsilon) - r^2\eta^2\log(\eta) \\ & + \epsilon^2\eta^2\log(\eta) - Br^2a_1 + B\epsilon^2a_1 + Ar^2\eta a_1 - A\epsilon^2\eta a_1 \\ & - 2B\eta^2\log(r)\,a_1 - 2A\eta^3\log(r)\,a_1 + 2B\eta^2\log(\epsilon)\,a_1 \\ & + 2A\eta^3\log(\epsilon)\,a_1)), \end{aligned} \tag{30}$$

$$\theta = \frac{\mathrm{J}_0(\frac{\eta\sqrt{\beta_s}}{\sqrt{a_2}})\mathrm{Y}_0(\frac{r\sqrt{\beta_s}}{\sqrt{a_2}}) - \mathrm{J}_0(\frac{r\sqrt{\beta_s}}{\sqrt{a_2}})\mathrm{Y}_0(\frac{\eta\sqrt{\beta_s}}{\sqrt{a_2}})}{\mathrm{J}_0(\frac{\eta\sqrt{\beta_s}}{\sqrt{a_2}})\mathrm{Y}(\frac{\epsilon\sqrt{\beta_s}}{\sqrt{a_2}}) - \mathrm{J}_0(\frac{\epsilon\sqrt{\beta_s}}{\sqrt{a_2}})\mathrm{Y}_0(\frac{\eta\sqrt{\beta_s}}{\sqrt{a_2}})}, \tag{31}$$

$$\phi = \frac{\mathrm{J}_0(\frac{i\eta\sqrt{Y}}{\sqrt{a_3}})\mathrm{Y}_0(-\frac{ir\sqrt{Y}}{\sqrt{a_3}}) - \mathrm{J}_0(\frac{ir\sqrt{Y}}{\sqrt{a_3}})\mathrm{Y}_0(-\frac{i\eta\sqrt{Y}}{\sqrt{a_3}})}{\mathrm{J}_0(\frac{i\eta\sqrt{Y}}{\sqrt{a_3}})\mathrm{Y}_0(-\frac{i\epsilon\sqrt{Y}}{\sqrt{a_3}}) - \mathrm{J}_0(\frac{i\epsilon\sqrt{Y}}{\sqrt{a_3}})\mathrm{Y}_0(-\frac{i\eta\sqrt{Y}}{\sqrt{a_3}})}. \tag{32}$$

where $a_1 = \frac{\mu_{nf}}{\mu_f}(1 + \frac{1}{\beta})$, $a_2 = \frac{\mathrm{k}_{nf}}{\mathrm{k}_f}$, $a_3 = \frac{\mathrm{D}_{nf}}{\mathrm{D}_f}$.

Here J_0 and Y_0 are the Bessel function of the first and second kinds, respectively.

4. Physical quantities

The formula for the flow rate $F(z)$ is

$$F(z) = \int_{\epsilon}^{\eta} r\,w\,dr. \tag{33}$$

Following the aforementioned integration calculation, the flow rate $F(z)$ can be expressed as follows:

$$F(z) = S_1\frac{dp}{dz} + S_2, \tag{34}$$

where

$$S_1 = -\epsilon^4\eta^2 + 2\epsilon^2\eta^4 - \eta^6 + \epsilon^4\eta^2\log(\epsilon) - \eta^6\log(\epsilon) - \epsilon^4\eta^2\log(\eta) + \eta^6\log(\eta) - B\epsilon^4 a_1 + A\epsilon^4\eta a_1 - 4A\epsilon^2\eta^3 a_1 + B\eta^4 a_1 + 3A\eta^5 a_1 + 4B\eta^4\log(\epsilon)\, a_1 + 4A\eta^5\log(\epsilon)\, a_1 - 4B\eta^4\log(\eta)\, a_1 - 4A\eta^5\log(\eta)\, a_1, \quad (35)$$

$$S_2 = -4\mathrm{w}_0\epsilon^2\eta^2 a_1 + 4\mathrm{w}_0\eta^4 a_1 + 8\mathrm{w}_0\eta^4\log(\epsilon)a_1 - 8\mathrm{w}_0\eta^4\log(\eta)\, a_1. \quad (36)$$

One can ascertain the outside wall's heat transfer coefficient by

$$\mathrm{HTC} = a_2\left(\frac{\partial R}{\partial z}\,\frac{\partial T}{\partial r}\right)\Big|_{r=R} = \frac{\frac{2a_2}{\pi\eta}\frac{d\eta}{dz}}{\mathrm{J}_0\left(\frac{\eta\sqrt{\beta_s}}{\sqrt{a_2}}\right)\mathrm{Y}_0\left(\frac{\epsilon\sqrt{\beta_s}}{\sqrt{a_2}}\right) - \mathrm{J}_0\left(\frac{\epsilon\sqrt{\beta_s}}{\sqrt{a_2}}\right)\mathrm{Y}_0\left(\frac{\eta\sqrt{\beta_s}}{\sqrt{a_2}}\right)}. \quad (37)$$

The following formula is used to calculate the shear stress at the stenotic wallwhere

$$WSS = -a_1\left(\frac{\partial w}{\partial r}\right)\Big|_{r=R} = \frac{\mathrm{w}_0 a_1\eta}{-Ba_1 + Aa_1\eta + \eta^2\log(\epsilon) - \eta^2\log(\eta)} - \frac{dp}{dz}\frac{(-4Ba_1\eta - \epsilon^2\eta + \eta^3 + 2\eta^3\log(\epsilon) - 2\eta^3\log(\eta))}{4(-Ba_1 + Aa_1\eta + \eta^2\log(\epsilon) - \eta^2\log(\eta))}.$$

5. Discussion on graphical exhibitions

This section discusses the significant effects of various rheological and geometrical parameters on blood flow with gold nanoparticles using graphs of thermal transfer coefficient, wall shear stress, velocity, thermal, and concentration profile.

Velocity profile

Figs. 2(a)–(c) serve as illustrations of how velocity behaves in a radial-directed stenotic artery. Fig. 2(a) shows the variation in velocity profile with the variation in the flow rate F. It was observed that with increasing F the velocity decreases in the interval 0 to 0.2, while in the interval 0.2 to 1 the velocity increases with increasing F. When the flow rate F increases, more blood is moving, which raises blood velocity, provided the cross-sectional area stays identical. As the ratio of the maximum height of the stenosis to the width of the channel δ and the shape parameter stenosis n increased, we scrutinized the same behavior. Fig. 2(b) exhibits the variation in velocity profile with the variation in the maximum depth of blood clot σ. It was observed that with increasing σ the velocity increasing in the interval 0 to 0.5 , while in the interval 0.5 to 1 the velocity decreasing with increasing σ. In terms of physical representation, it shows the extent or size of a clot inside the artery, which decreases the area of effective flow. By raising both the radius of catheter c and the nanoparticle volume fraction φ, we obtained the same pattern, but φ has a small impact. In physics, increasing the volume fraction of nanoparticles φ typically results in an increase in

viscosity, which can lower blood velocity if the overall flow rate is unaltered. Fig. 2(c) illustrates how the velocity profile changes as the second-order slip parameter B changes. It was noted that the velocity decreases with enhancing B in $0.2 \leq r \leq 0.7$, it increases by raising B in $0 \leq r \leq 0.2$ and in $0.7 \leq r \leq 1$. Similar behavior was observed by first-order slip parameter A and the slip velocity at the wall w_0 enlarge. Physically, the influence of wall friction is lessened as w_0 increases, enabling a rise in blood velocity in the areas nearest the wall.

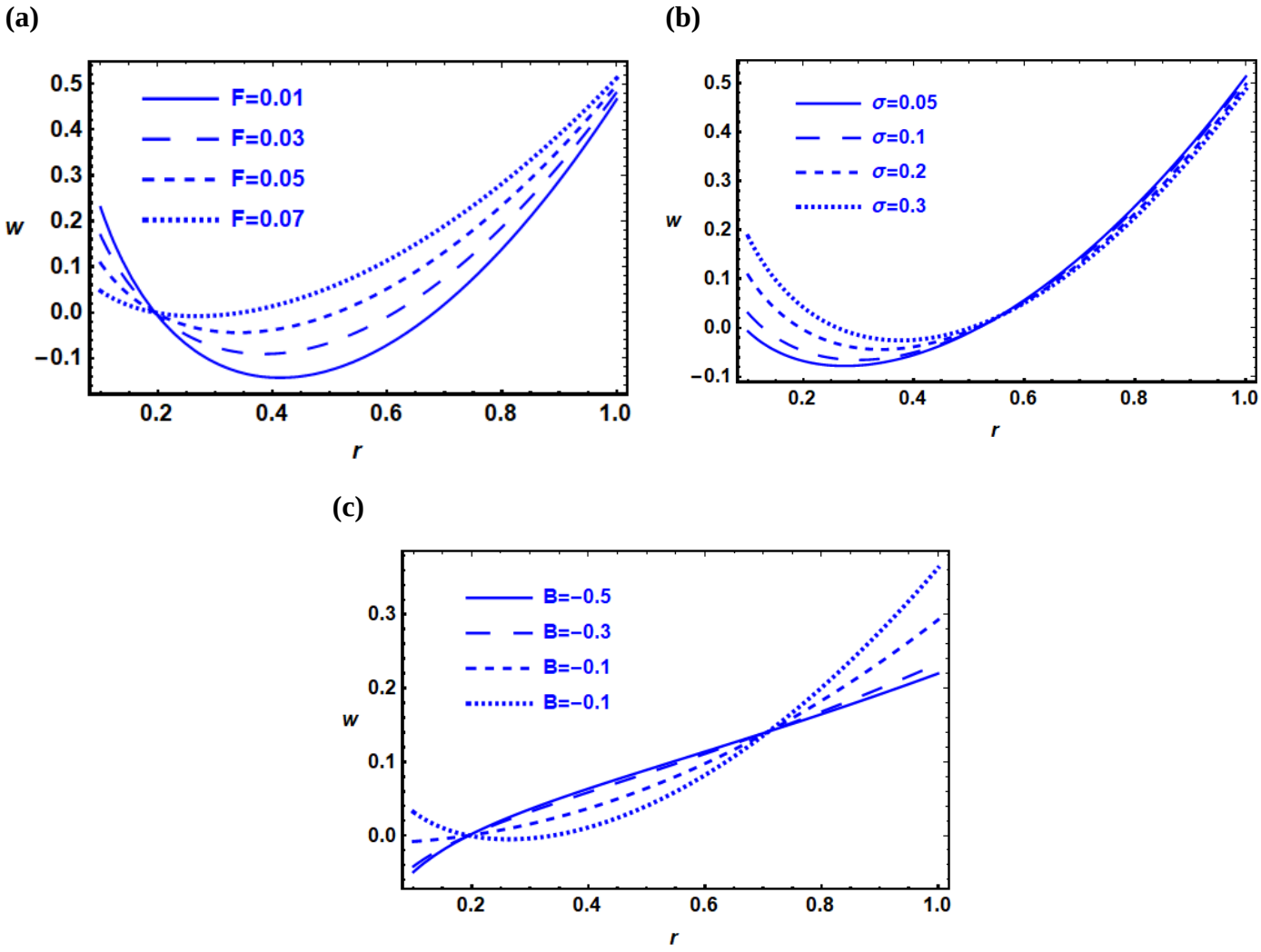

Fig. 2. Effect of (a) F, (b) σ, and (c) B on velocity.

Temperature profile

The temperature pattern in a radial-directed stenotic artery is demonstrated in Figs. 3(a)–(c). It is evident from Fig. 3(a) that an increase in the maximum depth of blood clot σ tends to cause the temperature graph to emerge. The temperature profile has the same manner as the radius of catheter c, the ratio of the maximal height of the stenosis to the channel width δ, and the thrombus's axial

displacement z_d rise. Fig. 3(b) reveals that the temperature profile enlarges by boosting the values of heat source parameter β_s due to the fact that metabolic processes inside the base fluid generate more heat. Heat source parameter β_s improves blood temperature, maintains blood viscosity, and facilitates blood circulation via the vessels, preventing clotting, elevating blood pressure, and other issues. The temperature profile for various values of the ratio of the maximum height of the stenosis to the channel width δ is shown in Fig. 3(c). The temperature profile has been shown to decrease when δ increases. As the stenosis shape parameter n grew, same behavior was seen.

.

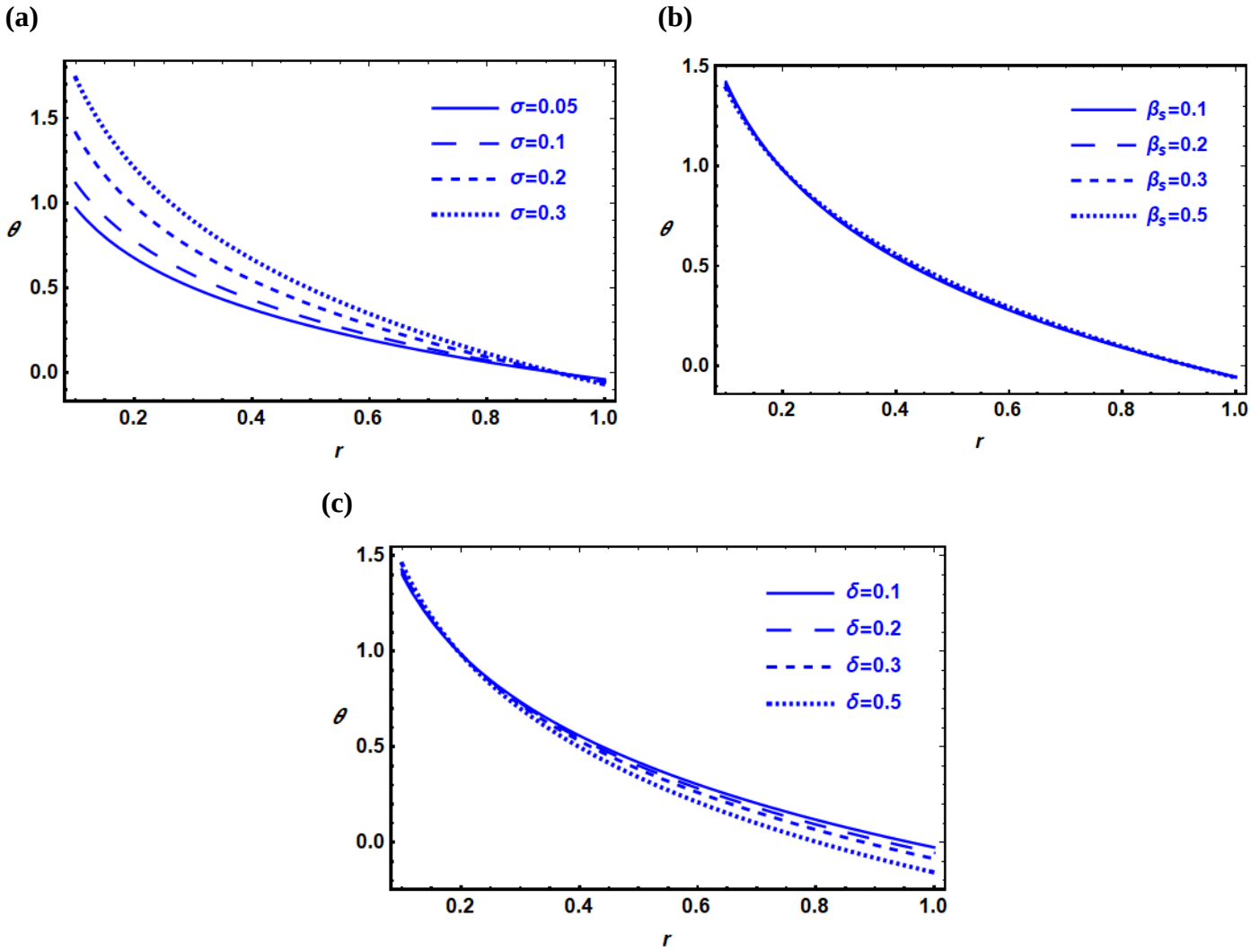

Fig. 3. . Effect of (a) σ, (b) β_s, and (c) δ on temperature.

Concentration profile

For the analysis of and chemical and physical systems in engineering applications, it is essential to comprehend how concentration varies with various parameters. A useful tool for visualizing

how different factors affect concentration rates and their dynamic manners is concentration distribution. Figs. 4(a)-(c) depict the concentration distributions of a nano-blood through the stenotic artery in the radial axis. In Fig. 4(a), the profile of concentration is illustrated for various values of the maximum depth of blood clot σ. A growth in the value of σ outcomes in an increase in the concentration distribution. Physically, an increased clot could potentially modify the flow layout and reduce resistance to the flow of blood, resulting in a lower concentration. As the radius of catheter c and the thrombus's axial displacement z_d increased, we scrutinized the same behavior. Fig. 4(b) reveals that the concentration varies non-linearly with the chemical reaction parameter γ, demonstrating both rising and falling portions that indicate complicated interactions. In Fig. 4(c), the concentration distribution is diagrammatically displayed for a variety of stenosis shape parameter n. Fig. 4(c) depicts the pattern of a decrease in the concentration of the nano-blood as the quantity of n increases.

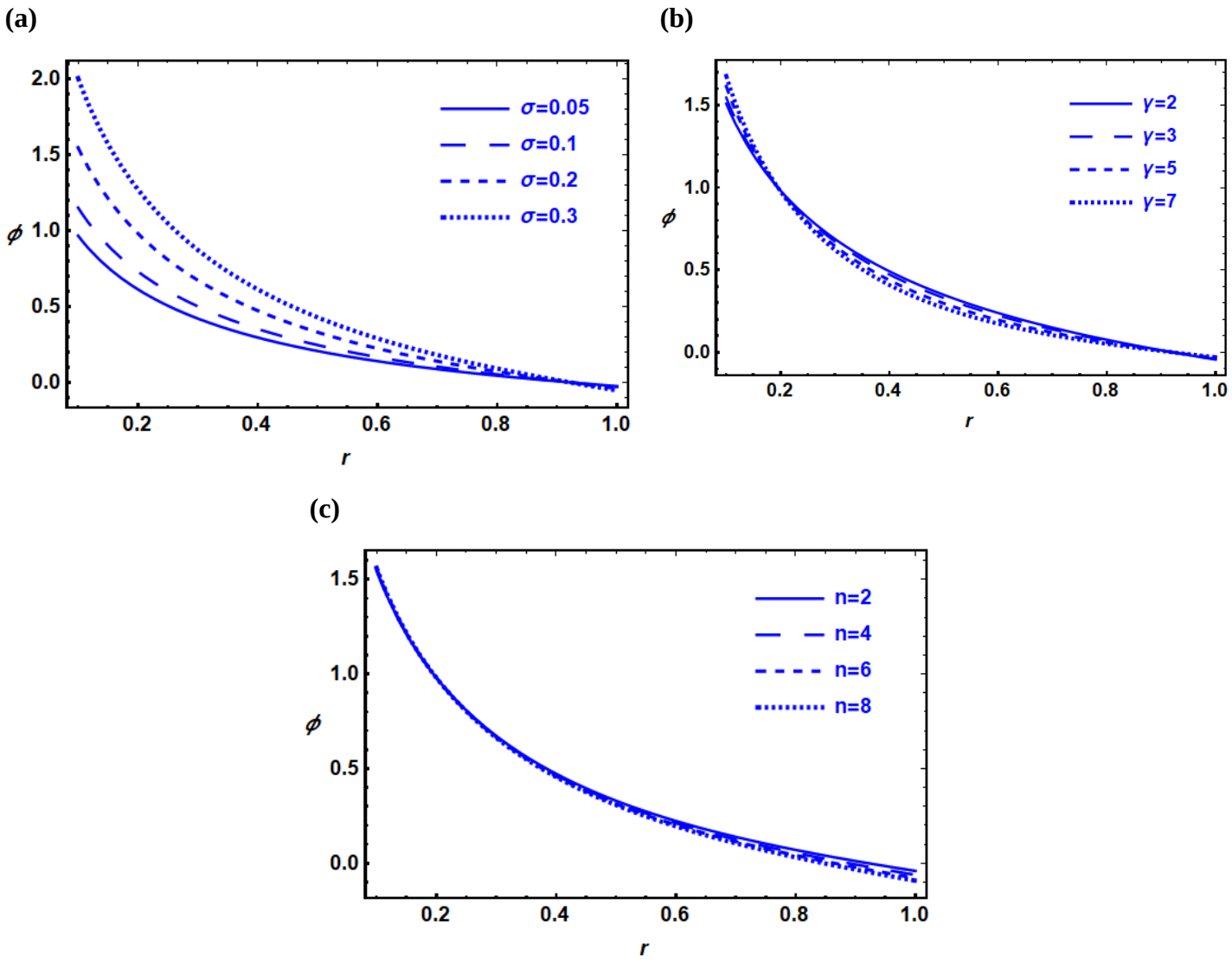

Fig. 4. Effect of (a) σ, (b) γ, and (c) n on concentration.

Heat transfer coefficient (HTC)

The HTC measures the rate of heat transmission between two surfaces or media: more efficient heat transmission results from a greater temperature gradient. In essence, heat is transferred from the blood to the arterial wall, the larger the temperature differential between the two, boosting the HTC. A fluid's capacity to transfer heat is gauged by its HTC. The HTC in an atherosclerotic artery affects the thermal stresses and temperature distribution inside the arterial wall, which impacts the stability and progression of plaque. The HTC is important for comprehending and controlling blood flow's thermal dynamics, particularly in medical settings where proper temperature control at the vascular walls is essential.

To illustrate radius of catheter c effect on the considered model, Fig. 5(a) shows the relation between HTC and radius of catheter c. Fig. 5(a) shows that HTC increases with c an increase in the region $0 \leq z \leq 0.5$. By raising c, the blood's temperature upsurges and the temperature differential between the blood and the arterial wall widens. The converse manner occurs in the region $0.5 \leq z \leq 1$. The HTC profile has the same manner as the heat source parameter β_s, the volume fraction of nanoparticles φ, and the ratio of the maximal height of the stenosis to the channel width δ rise.

As the maximum depth of blood clot σ rises in Fig. 5(b), HTC falls in the region $0.5 \leq z \leq 1$; otherwise, it exhibits the same pattern. Fig. 5(c) shows that in the region $0.3 \leq z \leq 0.8$, the HTC elevates with increasing values of the stenosis shape parameter n, however in the other region, it declines. Physically, the thin section's constriction effect intensifies with growing n, which could result in more variations in pressure and, in turn, the distribution of temperature. Fig. 5(d) exhibits that the same trend was emerged in accordance with Fig. 5(c) when the values of the thrombus's axial displacement z_d are altered. This figure shows a shift in the temperature distribution at various points inside the artery because of changes in the blood flow patterns and heat distribution surrounding the clot as the clot displacement boosts.

(a)

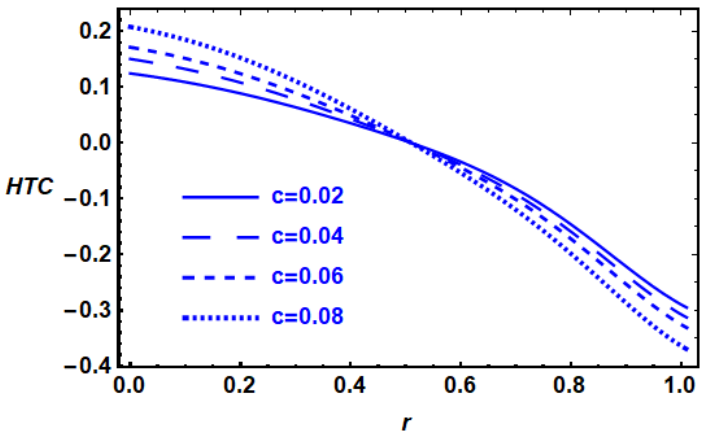

(b)

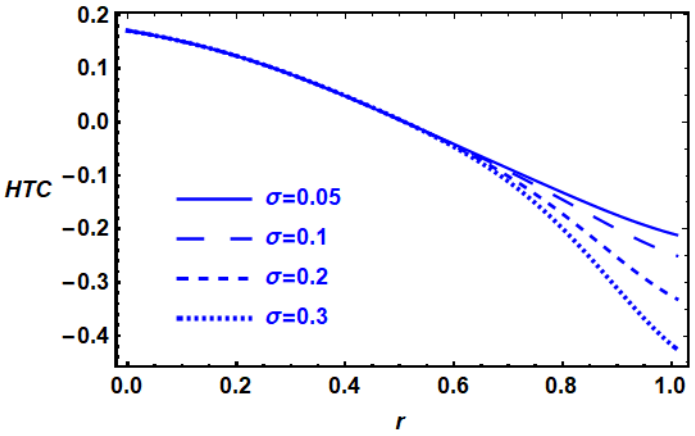

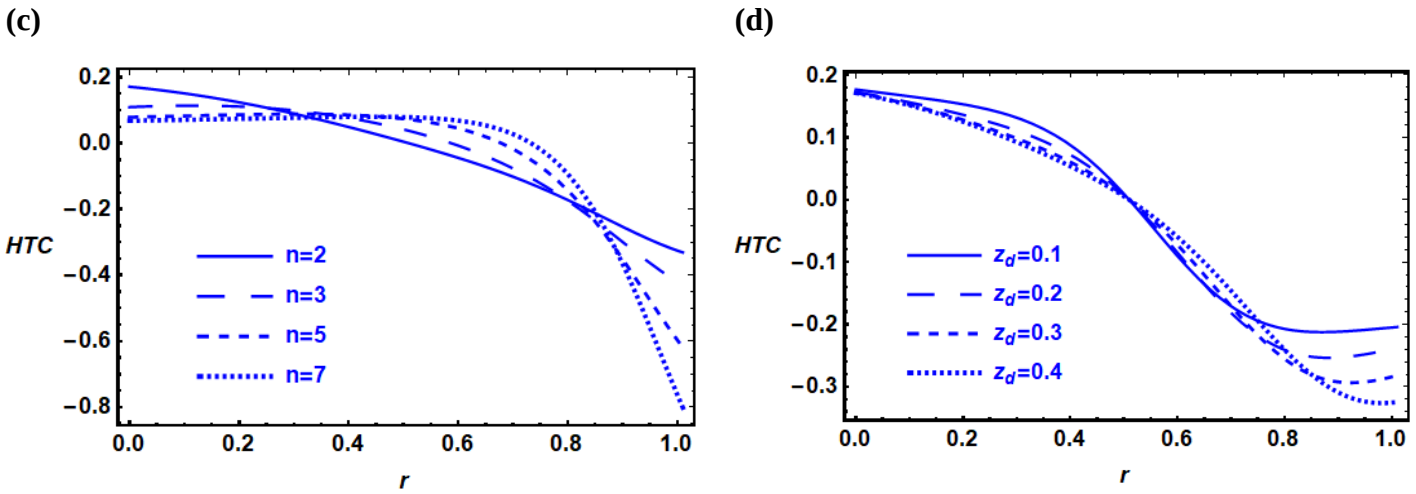

Fig. 5. Effect of (a) c, (b) σ, (c) n, and (d) z_d on HTC.

Wall shear stress (WSS)

Resistance arises between the fluid and solid when the fluid enters the solid-solid interaction because the fluid is moving and the solid is immobile. It is crucial to assess the amount of shearing that occurs between the fluid and solid surfaces during fluid movement. Because of the close relationship between the location of arteriosclerosis and the wall of a blood vessel, WSS is especially important for comprehending the development of arterial disorders.

As the second slip B parameter and the volume fraction of nanoparticles φ increase, the magnitude of WSS decreases, as seen in Figs. 6(a) and 6(b). Additionally, a reverse and identical response is seen when the slip velocity at the wall w_0 and the first slip parameter A are expanded, respectively. Figs. 6(c) and 6(d) show the WSS distribution for various values of the maximum stenosis height to the flow rate F and the channel width δ. Increasing the values of F and δ is observed to increase the WSS's magnitude. Increased WSS magnitudes in certain regions and modifications in blood flow patterns are caused by enlarging δ.

In Figs. 6(e) and 6(f), the WSS profile is shown for different values of radius of catheter c and stenosis shape parameter n. It is noted that the WSS curves show a significant decrease when c and n values rise, while the reverse impact is seen as z increases. The same c, but with a lesser effect, is produced by increasing the maximum depth of blood clot σ while increasing z_d results in the opposite effect.

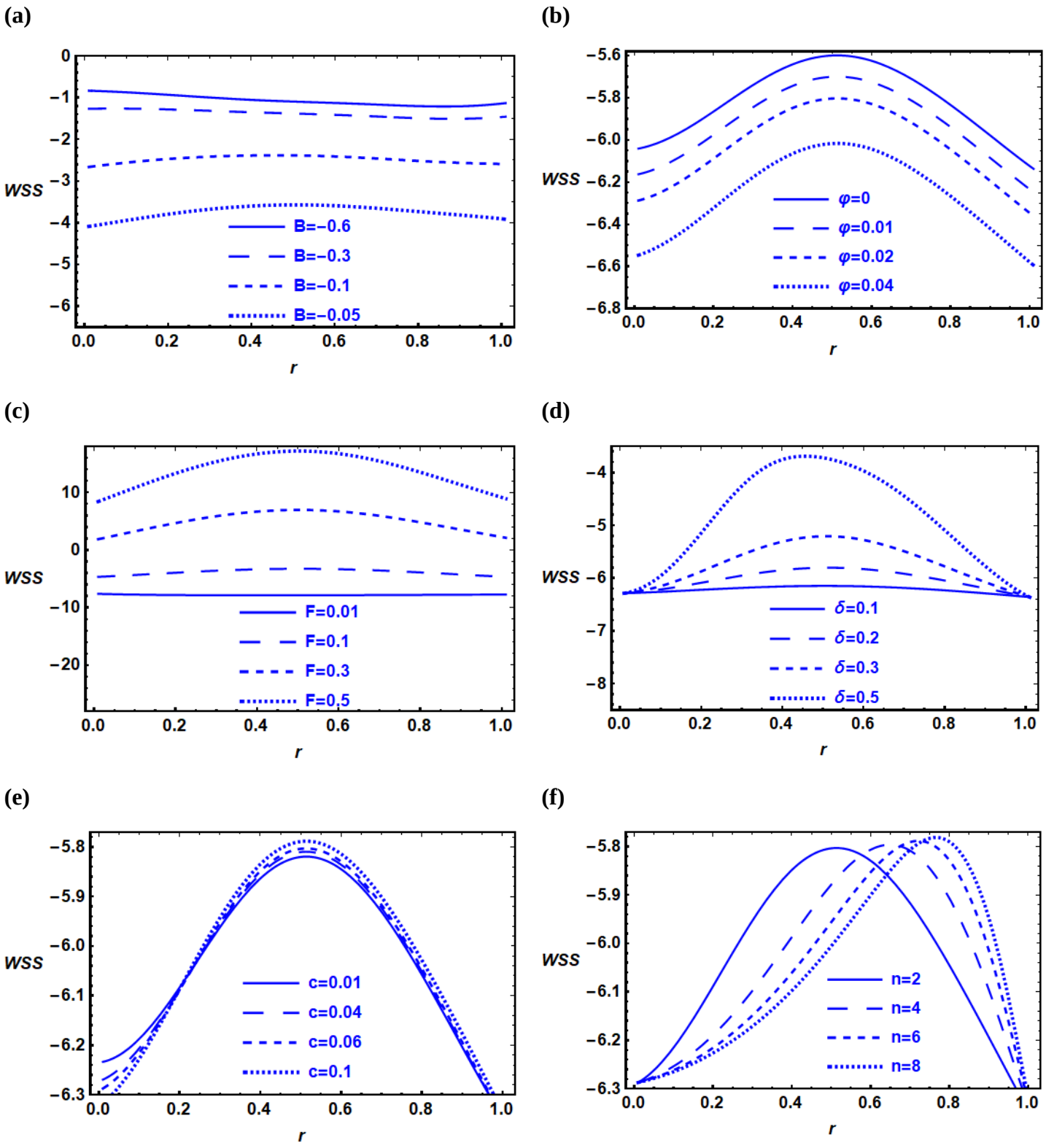

Fig. 6. Effect of (a) B, (b) φ, (c) F, (d) δ, (e) c, and (f) n on WSS.

6. Conclusions

In this project, we constructed mathematical models to study the properties of blood flow through a constricted artery with a catheter that contains Au-nanoparticle. Differential equations governing the fluid's temperature, velocity, and concentration were used to express these models. The software Mathematica 14.1 was used to solve these problems analytically. Below is a summary of the key findings:

- Velocity is affected in the same way by parameters B, A, and w_0.
- Heat source parameter β_s improves blood temperature.
- Both rising and falling segments that show complex interactions have occurred in the concentration, which fluctuates nonlinearly with the chemical reaction parameter γ.
- The impact of β_s, φ, δ, and c on the rise and decrease of heat transmission is equivalent.
- The magnitude of WSS diminishes as φ and B rise.

The findings of this study may have significant ramifications for bettering medication delivery systems, treating cardiovascular disorders, and comprehending how blood flows in stenosed arteries. It also emphasizes how important nanotechnology is to contemporary medicine and how it may help patients with vascular illnesses.

References

1. M. Keane, M. O'Toole (2003). Miller-Keane Encyclopedia and Dictionary of Medicine (7th edition). Nursing & Allied Health, Elsevier.
2. L. Sherwood (2016). Human physiology: From cells to systems, Cengage Learning, USA.
3. E. Kuzma, I. Lourida, S. F. D. Moore (2018). Stroke and dementia risk: A systematic review meta-analysis. Alzheimer's & Dementia.11 1416-1426.
4. H. Kanai, M. Iizuka, K. Sakamoto (1970). One of the problems in the measurement of blood pressure by catheter-insertion: Wave reflection at the tip of the catheter. Medical and biological engineering 8 (5) 483-496.
5. J. Tripathi, B. Vasu, O. A. Bég, R. S. R. Gorla, P. K. Kameswaran (2021). Computational simulation of rheological blood flow containing hybrid nanoparticles in an inclined catheterized artery with stenotic, aneurysmal and slip effects. Computers in Biology and Medicine 139 105009.
6. A. M. Zidan, L. B. McCash, S. Akhtar, A. Saleem, A. Issakhov, S. Nadeem (2021). Entropy generation for the blood flow in an artery with multiple stenosis having a catheter. Alexandria Engineering Journal 60 (6) 5741-5748.
7. S. Rathore, D. Srikanth. (2022). Mathematical study of transport phenomena of blood nanofluid in a diseased artery subject to catheterization. Indian Journal of Physics 96 (7) (2022) 1929-1942.

8. C. S. Sravanthi (2020). Second order velocity slip and thermal jump of Cu–water nanofluid over a cone in the presence of nonlinear radiation and nonuniform heat source/sink using homotopy analysis method, Heat TransferHeat Transfer-Asian Research 49 (1) 86-102.
9. J. Zhu, D. Yang, L. Zheng, X. Zhang (2016). Effects of second order velocity slip and nanoparticles migration on flow of Buongiorno nonanofluid. Applied Mathematics Letters 52 183–191.
10. M. H. M. Yasin, A. Ishak, I. Pop (2017) Boundary layer flow and heat transfer past a permeable shrinking surface embedded in a porous medium with a second-order slip: A stability analysis. Applied Thermal Engineering 115 1407–1411.
11. A. Majeed, F. M. Noori, A. Zeeshan, T. Mahmood, S.U. Rehman, I. Khan (2018). Analysis of activation energy in magnetohydrodynamic flow with chemical reaction and second order momentum slip model. Case Studies in Thermal Engineering 12 765–773.
12. A. Sahoo, R. Nandkeolyar (2023). Entropy generation in magnetohydrodynamic radiative non-Darcy slip flow of a Casson nanofluid with Hall effects and activation energy. Journal of Magnetism and Magnetic Materials 575 170712.
13. H. M. Sayed, E. H. Aly, M. M. Tharwatb, A. M. Mahros (2024). Melting heat transfer and entropy analysis of ternary Casson nanofluids flow with second slip conditions: Application on rocket engine cooling. Alexandria Engineering Journal 102 10–25.
14. U. S. Choi (1995). Enhancing thermal conductivity of fluids with nanoparticles, developments and application of non-Newtonian flows. ASME Journal of Heat Transfer 66 99-105.
15. C. E. Nsofor (2008). Recent patents on nanofluids (nanoparticles in liquids) heat transfer. Recent Patents on Mechanical Engineering 1 (3) 190–7.
16. Z. Guo (2020). A review on heat transfer enhancement with nanofluids, Journal of Enhance. Heat Transfer 27 (1) 1–70.
17. B. Prasad, R. Bali (2023). Mathematical study of nanoparticle loaded in red blood cells for drug delivery in an artery with stenosis. Physics of Fluids 35 091902.
18. P. Paul, S. Das (2023). EDL flow designing of an ionized Rabinowitsch blood doped with gold and GO nanoparticles in an oblique skewed artery with slip events. BioNanoScience 13 2307–2336.
19. J. Iqbal, F.M. Abbasi (2025). Integration of artificial neural network computing for radially magnetized bioconvection peristaltic movement of Reiner-Philippoff nanofluid with porous medium. Journal of Molecular Liquids 419 126783.
20. S. E. Ghasemi, A. A. Ranjbar (2025). Peristaltic nanofluid flow analysis inside wavy channels for pharmacological applications. Results in Chemistry 14 102128.
21. N. Casson (1959). A flow equation for pigment-oil suspensions of the printing ink type. In: Mill, C.C., Ed., Rheology of Disperse Systems, Pergamon Press, Oxford. 84-104.
22. G. W. S. Blair (1959). An equation for the flow of blood, plasma and serum through glass capillaries. Nature 183 (4661) 613–614.
23. A. L. Copley (1960). Apparent viscosity and wall adherence of blood systems, in Flow Properties of Blood and Other Biological Systems, A. L. Copley and G. Stainsly, Eds., Pergamon Press,Oxford, UK.

24. B. K. Sharma, R. Gandhi, T. Abbas, M. M. Bhatti (2023). Magnetohydrodynamics hemodynamics hybrid nanofluid flow through inclined stenotic artery. Applied Mathematics and mechanics (english edition) 44 (3) 459–476.
25. V. Dhinakaran, K. D. Anuradha, J. U. Viharika, U. Khan, N. Abdullah, S. Elattar (2025). Effectiveness of heat source/sink and Lorentz force constraints in a non-Newtonian peristaltic arterial blood hybrid nanofluid past an overlapping stenotic artery. Case Studies in Thermal Engineering 65 105577.
26. M. Fahim, M. Sajid, N. Ali, M. N. Sadiq (2023). Heat and mass diffusion to Williamson fluid streaming through tube with multiple stenosis while subjected to periodic body acceleration. Mathematical Modelling of Natural Phenomena 18 19
27. T. Elnaqeeb (2019). Modeling of Au(NPs)-blood flow through a catheterized multiple stenosed artery under radial magnetic. The European Physical Journal Special Topics 228 2695-2712.